High-Coverage Structures of Carbon Monoxide Adsorbed on Pt(111) Studied by High-Pressure Scanning Tunneling Microscopy†

Sarah R. Longwitz,‡,§ Joachim Schnadt,‡ Ebbe Kruse Vestergaard,‡ Ronnie T. Vang,‡ Erik Lægsgaard,‡ Ivan Stensgaard,‡ Harald Brune,§ and Flemming Besenbacher*,‡

Interdisciplinary Nanoscience Center (iNANO) and Department of Physics and Astronomy, University of Aarhus, 8000 Aarhus C, Denmark, Institut de Physique des Nanostructures, Ecole Polytechnique Fédérale de Lausanne, 1015 Lausanne, Switzerland

Received: February 20, 2004

High-pressure scanning tunneling microscopy was used to study the room-temperature adsorption of CO on a Pt(111) single-crystal surface in equilibrium with the gas phase. The coverage was found to vary continuously, and over the entire range from 10^{-6}−760 Torr pressure-dependent moiré patterns were observed, characteristic of a hexagonal or nearly hexagonal CO overlayer. Two different pressure ranges can be distinguished: below 10^{-2} Torr, the moiré lattice vector is oriented along a 30° high-symmetry direction of the substrate, corresponding to a pressure-dependent rotation of the CO overlayer with respect to the (1 × 1) Pt surface lattice, while above 10^{-2} Torr, the CO layer angle is independent of the pressure. This behavior is analyzed in terms of the interplay of the repulsive CO−CO interaction potential and the substrate potential.

Introduction

Few adsorbate systems have received as much attention as carbon monoxide on transition-metal surfaces. The enormous interest originates from the system's relevance to catalysis, since CO takes part in many important reactions such as CO hydrogenation and oxidation and the Fischer-Tropsch synthesis[1] and transition-metal particles are the most common catalytic materials for these reactions. Notwithstanding these beneficial interactions, carbon monoxide is also an unwanted poison molecule in, e.g., the hydrogen feed for low-temperature fuel cells produced from hydrocarbons.[2] Since all these aspects can be traced back to adsorbate−surface interactions, it is important to acquire a thorough understanding of the properties of the adsorption of CO on transition-metal surfaces.

To date, an impressively detailed knowledge has been gained on the adsorption of CO on Pt(111) under ultrahigh vacuum (UHV) conditions (see, e.g., refs 3, 4, and 5). The relevance of this understanding to industrial catalytic conditions has however been questioned.[6,7] The divergence of experimental and theoretical results for systems under UHV and catalytic or realistic pressures, respectively, has been designated "the pressure gap", which has to be bridged (see, e.g., ref 8). Therefore the development of surface-sensitive techniques that are capable of working at elevated pressures has renewed the interest in the CO/Pt(111) system, and a number of recent high-pressure studies have addressed the subject using different techniques.[6,7,9,10] These studies revealed that carbon monoxide forms a hexagonal overlayer on Pt(111) at atmospheric pressure and room temperature. Two different structures were proposed, one close to a (4 × 4)-9CO nonrotated structure,[7] the other one compatible with a ($\sqrt{19} \times \sqrt{19}$) R23.4°-13CO commensurate structure.[10] The latter structure has also been proposed for the adsorption of CO in an electrochemical cell at 0−0.2 V electrode potential.[11] In contrast, under UHV and low-temperature conditions, a series of nonhexagonal commensurate structures is observed.[3,4,12] These are the c(4 × 2) or ($\sqrt{3} \times 2$)rect ($\theta = {}^1/_2$, where θ is the coverage (ref 13)) and c($\sqrt{3} \times 5$)rect ($\theta = {}^3/_5$), ($\sqrt{3} \times 3$)rect ($\theta = {}^2/_3$), and c($\sqrt{3} \times 7$)rect ($\theta = {}^5/_7$) structures; the latter three can be cast in a unified picture in which unit stripes of the c(4 × 2) structure separated by domain walls of higher, structure-specific CO density.[4] It is not yet clear, however, whether these lattice gas structures represent global or local minima of the potential energy surface.

While it was shown that a hexagonal CO overlayer can also be produced under vacuum conditions when the sample is cooled sufficiently,[3,10] the understanding of the atomic-scale details of the room-temperature adsorption structures of CO on Pt(111) over the entire pressure range from UHV pressures up to atmospheric pressure is still incomplete. In particular, no study has been able to unambiguously determine the adsorbate structure for the complete pressure range from UHV to one atmosphere.

For the present study we used high-resolution scanning tunneling microscopy (STM) to unravel the room-temperature adsorption structures of CO/Pt(111). At all pressures above 10^{-6} Torr, we observed moiré patterns characteristic of the formation of a hexagonal CO overlayer on the hexagonal Pt(111) surface. The superposition of the two hexagonal lattices leads to a beating phenomenon resulting in the moiré pattern. A one-dimensional analogy is given by the sum of two sine functions with slightly different frequencies. At low CO pressures, up to 10^{-2} Torr, the moiré pattern is characterized by a lattice vector oriented along one of the high-symmetry directions of the substrate, while at higher CO pressures, a rotation of the pattern is observed. In the following, we discuss these results in the context of existing theories and compare them to available UHV low-temperature data and results obtained in electrochemical cells.

Experimental Section

The experiments were performed in a UHV chamber equipped with a home-built Aarhus scanning tunneling microscope as well as UHV standard equipment for sample cleaning and charac-

† Part of the special issue "Gerhard Ertl Festschrift".

* To whom correspondence may be addressed. E-mail: fbe@phys.au.dk.
‡ University of Aarhus.
§ Ecole Polytechnique Fédérale de Lausanne.

10.1021/jp0492218 CCC: $27.50
Published on Web 06/05/2004

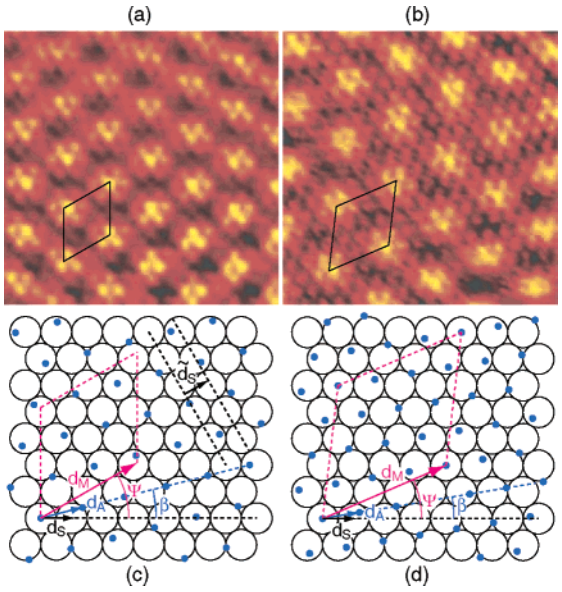

Figure 1. STM images of 55 × 55 Å^2 and corresponding ball models showing moiré superstructures of CO on Pt(111) at room temperature. (a) Incommensurate structure at $p = 10^{-2}$ Torr, $I_t = 1.06$ nA, $V_t = 8.2$ mV. (b) $p = 720$ Torr, $I_t = 1.27$ nA, $V_t = 4.9$ mV. The images a and b are aligned so that the bulk [1$\bar{1}$0] direction is oriented along the x axis. The image treatment comprised frequency filtering and interpolation. In the ball models in c and d, the open circles represent Pt atoms and the dark blue dots CO molecules. The rotational angles β between the substrate and adsorbate lattices and Ψ between the substrate and moiré lattices are indicated. The moiré unit cell with lattice constant d_M is also shown. (c) Incommensurate structure at 10^{-2} Torr. $\Psi = 30°$, $\beta = 10.4°$, $d_M/d_S = 3.6$. $\vec{\tilde{d}}_S$ is the real space equivalent of the reciprocal vector $\vec{\tilde{q}}_S$ observed in the fast Fourier transform (cf. Figure 2). $\vec{\tilde{d}}_S$ is rotated by 30° from $\vec{d}_S$, and the length relationship is $\tilde{d}_S = \sqrt{3}d_s/2$. (d) Commensurate ($\sqrt{19} \times \sqrt{19}$) R23.4°-13CO structure at 720 Torr. $\Psi = 23.4°$, $\beta = 9.5°$, $d_M/d_S = 4.4$.

terization.[14] Connected to this chamber is a gold-plated cell containing the newly developed Aarhus high-pressure scanning tunneling microscope.[15] With this, STM experiments can be carried out at pressures of up to 760 Torr of pure gases or gas mixtures. Sample transfer between the systems takes place under clean conditions, i.e., without removing the sample from the vacuum. The gas exposure system of the high-pressure cell has been designed to avoid nickel-carbonyl ($Ni(CO)_4$) formation, which is of utmost importance when working with CO. For that purpose, the gas line has been constructed primarily using copper tubing instead of stainless steel. Furthermore, just prior to the inlet, the CO is passed through an activated high surface area carbon powder filter heated to ~400 K, over which the Ni-carbonyls dissociate, leaving the Ni behind. The efficiency of this system was checked by performing Auger electron spectroscopy after extended high-pressure CO exposure and subsequent pump-out.

The sample was cleaned in the UHV chamber following standard sample cleaning procedures: 30 min 800 eV Ar^+ sputtering, followed by an annealing procedure (in case of severely contaminated samples, 10 min annealing at 800 K in 10^{-7} Torr O_2 plus 3 min annealing at 1000 K in UHV, otherwise just UHV anneal). The experiments at low and medium pressure (up to 5×10^{-4} Torr) were then performed in the UHV chamber, while those at higher pressures up to 760 Torr were performed in the high-pressure cell. For pressures between 0.1 and 100 Torr, electric discharges between the closely spaced piezo electrodes may occur. We thus always work at a total pressure of close to 760 Torr in the high-pressure cell. Because of its unreactive nature, ultrapure argon as commercially available is used for backfilling from the desired CO pressure up to the working pressure.

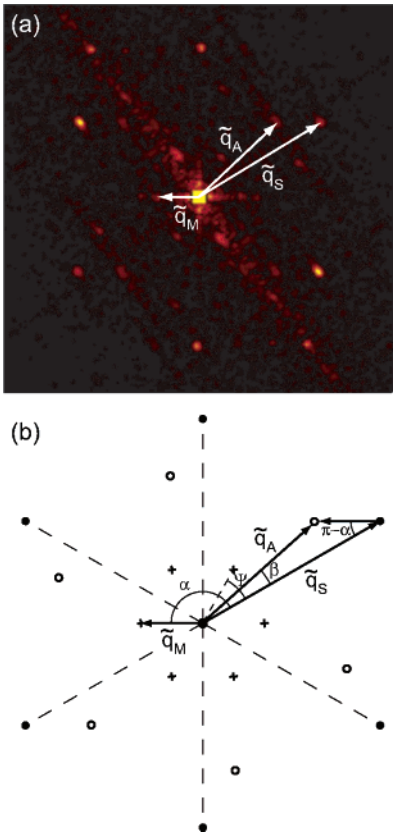

Figure 2. (a) FFT of an STM image of a CO/Pt(111) moiré pattern (5×10^{-7} Torr). (b) Relationship between the reciprocal lattice vectors. Here the filled circles represent the substrate lattice, the empty circles correspond to the adsorbate lattice, and the crosses correspond to the resulting moiré pattern. The observed vectors $\vec{\tilde{q}}_M$, $\vec{\tilde{q}}_S$, and $\vec{\tilde{q}}_A$ are rotated by 30° from the vectors $\vec{q}_M$, $\vec{q}_S$, and $\vec{q}_A$ used in the analysis, and the vector lengths are related via $\tilde{q}_x = 2q_x/\sqrt{3}$, where x = M, S, A. The moiré vector $\vec{\tilde{q}}_M$ is equal to the difference vector $\vec{\tilde{q}}_M = \vec{\tilde{q}}_A - \vec{\tilde{q}}_S$ and hence also $\vec{q}_M = \vec{q}_A - \vec{q}_S$.

Results

Figure 1 shows two typical STM images of CO adsorbed on Pt(111) at room temperature. Image a was recorded at a CO pressure of 10^{-2} Torr, image b at 720 Torr. In both images, two hexagonal structures coexist, one with a short and one with a longer periodicity. The short-periodicity hexagonal lattice is the image of either the Pt(111) substrate (panel a) or the CO overlayer (panel b), while the long-periodicity lattice (the moiré lattice) is characterized by the periodic height modulation induced by the superposition of the hexagonal CO adsorbate layer and the Pt(111) surface.[16] Similar images, all of which exhibited moiré patterns, were obtained at the other investigated pressures.

We observed quite generally that we could not image the CO molecules at pressures below 0.1 Torr (at room temperature), but instead we sampled the underlying Pt(111) substrate, as in Figure 1a. The measurement of the moiré pattern with a hexagonal shape, however, proves the presence of a hexagonal CO overlayer. The invisibility of CO adsorbed on Pt and other metal surfaces in STM is known to occur under certain conditions (see, e.g., refs 18, 19, and 20).

Performing fast Fourier transforms (FFT) on the STM images allowed us to measure the periodicities and angles of the

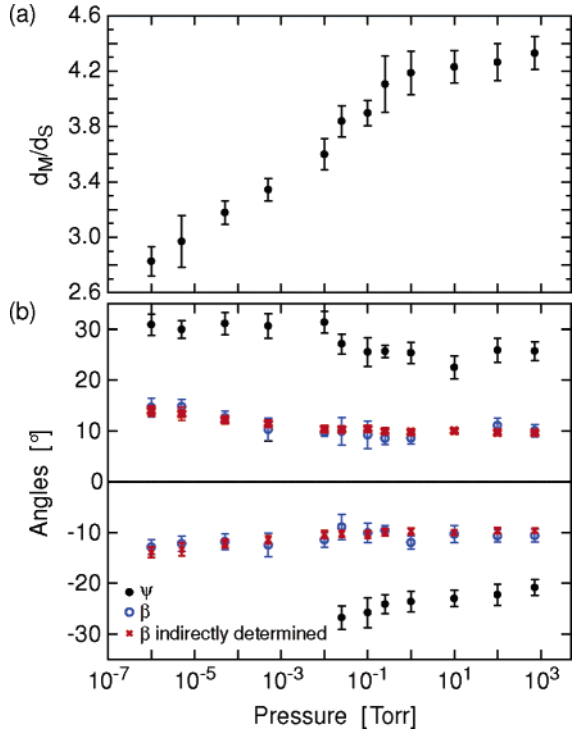

Figure 3. (a) Moiré lattice constant d_M for a CO layer on Pt(111) as a function of CO partial pressure. d_M is normalized with respect to the substrate lattice constant d_S. (b) Rotational angles between the substrate and the moiré lattice Ψ (filled symbols) and the substrate and adsorbate lattice β (open symbols). β can also be calculated from d_M, d_S, and Ψ (crosses).[21] In those cases, where two equivalent domains were observed (rotation of the moiré and adsorbate lattices by $\pm\Psi$ and $\pm\beta$ with respect to the substrate [1$\bar{1}$0] direction, respectively), the angles for both domains are given.

observed structure. A typical FFT is shown in Figure 2a, and a sketch of the relevant parameters is shown in Figure 2b. These are the reciprocal lattice vectors $\vec{\tilde{q}}_M$ of the moiré lattice, $\vec{\tilde{q}}_A$ of the adsorbate lattice, and $\vec{\tilde{q}}_S$ of the substrate lattice, which are related to each other by virtue of $\vec{\tilde{q}}_M = \vec{\tilde{q}}_A - \vec{\tilde{q}}_S$. This set of reciprocal vectors $\vec{\tilde{q}}_x$ translates into the set $\vec{q}_x$ (x = M, S, A), where $\vec{q}_x$ are the reciprocal space vectors of the real space vectors $\vec{d}_x$ used in Figure 1 and in the analysis below, by a rotation of 30° and by virtue of $\tilde{q}_x = 2q_x/\sqrt{3}$. Hence $\vec{q}_M = \vec{q}_A - \vec{q}_S$. Ball models showing the real space vectors are given in panels c and d of Figure 1. $\vec{d}_M$ and $\vec{d}_A$ form angles Ψ and β, respectively, relative to the [1$\bar{1}$0] direction of the substrate. From Figure 2a, it is seen that the adsorbate lattice vector can be determined even if the adsorbates are not visible in the STM image, since the moiré spots appear as satellites around the substrate spots.[21] The substrate spots can be identified unambiguously by comparison to the Fourier transforms of images taken on the clean Pt(111) crystal.

Figure 3 shows these parameters as a function of the CO partial pressure ranging from 10^{-6} to 760 Torr. In panel a, the moiré superlattice constant d_M is plotted in units of the Pt(111) substrate nearest neighbor distance $d_S = 2.77$ Å. In panel b, the filled circles refer to the rotation angle Ψ between the substrate and moiré lattice and the open circles to the rotation angle β between the substrate and adsorbate lattice. In addition, crosses indicate values for β which were derived from the moiré parameters only as described in ref 21. The procedure proved to be useful in case of barely visible satellites and gave additional confidence, since these values coincide with the β values determined directly from the images within the measurement uncertainty. From Figure 3b, we can identify two regimes

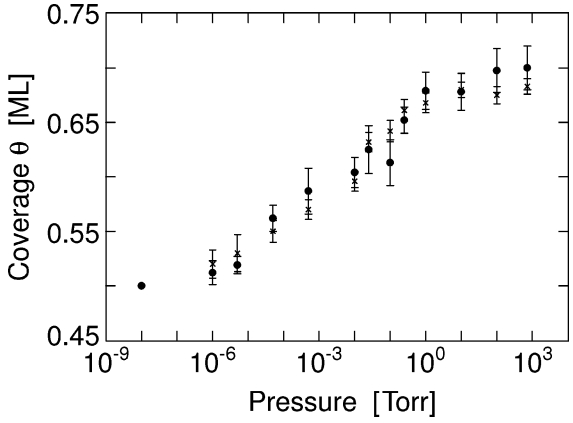

Figure 4. CO coverage θ on Pt(111) as a function of CO background pressure. The filled circles indicate values, which were directly determined from the STM images, while the indirectly determined values[21] are indicated by crosses.

with different types of incommensurate moiré superstructures. In the pressure range from 10^{-6} to 10^{-2} Torr, we observe a moiré pattern, which is rotated by a fixed angle of $\Psi = 30°$ with respect to the Pt(111) substrate, whereas the adsorbate angle β decreases from about 14 to 10°. At the same time, the lattice constant of the moiré pattern changes approximately linearly with the logarithm of the CO pressure. At CO pressures above 10^{-2} Torr, Ψ decreases, while β remains approximately constant at about 10°. Close to atmospheric pressure, the moiré lattice constant d_M approaches a fixed saturation value.

In panels c and d of Figure 1, a schematic model of the CO structures observed at 10^{-2} and 720 Torr is given. The ball model in panel c was created with the Ψ, d_M, d_A, and β values from the measurement. The structure at 720 Torr is compatible with a $(\sqrt{19} \times \sqrt{19})$ R23.4°-13CO commensurate structure, and the corresponding values were used in panel d.

Knowledge of the substrate and adsorbate lattice constants allows one also to determine the CO coverage, which is given by $\theta = (d_S/d_A)^2 = (q_A/q_S)^2$. Figure 4 shows how the coverage increases continuously with CO pressure in the range of 10^{-8}–10^3 Torr. Toward atmospheric pressures, the CO coverage saturates due to the increasingly repulsive CO−CO interaction. We confirmed that the variation of the CO coverage was reversible by first exposing the sample to a CO pressure of 760 Torr and then adjusting the pressure to a lower value. The structural parameters were the same as for a sample that was exposed to the lower pressure only. The results for the CO coverage are in good agreement with the previously determined CO coverages at 10^{-8} Torr ($\theta = 0.5$)[3] and 760 Torr ($\theta = 0.68$).[10] The CO coverage given for 10^{-8} Torr corresponds to the c(4 × 2) structure observed in low-energy electron diffraction (LEED).[3,22]

Discussion

From Figure 4, the coverage of CO on Pt(111) at room temperature is seen to vary continuously (and reversibly, as outlined above) over the pressure range from 10^{-6} to 760 Torr. The observed CO structures were hexagonally ordered. The finding of a continuous variation of the CO coverage with pressure and the observation of hexagonal, ordered overlayer structures for all pressures above 10^{-6} Torr is in contrast to the CO/Pt(111) lattice gas structures found in the same coverage range at lower pressures and temperatures.[3,4,12] The formation of lattice gas structures would lead to a phase diagram with alternating regimes of ordered and disordered CO overlayers.[4]

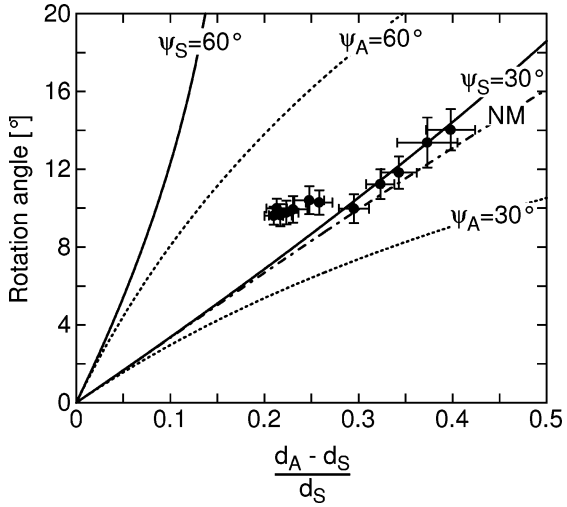

Figure 5. Rotation angle between CO adsorbate layer and Pt(111) substrate as a function of the lattice misfit between d_A and d_S, $(d_A - d_S)/d_S$. The solid and short-dashed lines indicate the theoretical high-symmetry solutions of ref 35 and the dashed−dotted line marked NM the harmonic approximation of ref 29 for a Lennard-Jones system. Ψ_S is the rotation angle of the moiré superlattice with respect to the substrate. Ψ_A is the rotation angle of the moiré superlattice with respect to the adsorbate.

Nevertheless, a true pressure gap is not observed for the CO/Pt(111) system since cooling of the sample to approximately 170 K leads to an increase in CO coverage and the formation of a hexagonal CO overlayer similar to that at 760 Torr.[10]

The formation of moiré structures has been observed previously for a large variety of adsorbate systems. For example, moiré patterns for CO overlayers have been reported for the Ni(111),[23] Ag(111),[24] and graphite[25] substrates and, at a pressure of ∼760 Torr, also for the CO/Pt(111) system.[7,10] Generally, the occurrence of moiré patterns can always be expected when the adsorbate lateral repulsive potential V_l balances or exceeds the corrugation ΔU of the adsorbate−substrate interaction potential. In the $V_l \gg \Delta U$ and infinite lattice limit, the resulting structure can be viewed as a mere superposition of two perfect, in this case hexagonal, lattices of the substrate and adsorbate, respectively. Because of the small difference in the adsorbate and substrate lattice constants, a long-periodicity (given by the moiré wave vector) height modulation is then observed.[16]

In the case $V_l \approx \Delta U$, the situation is more complicated and has received considerable theoretical interest.[26−36] The various theories predict an alignment of the moiré vector in preferred directions if the molecules are able to relax their positions with respect to the perfect hexagonal overlayer lattice[26−32] and/or if the system has a finite size.[33−36] References 33−36 put forward a "high-symmetry hypothesis" according to which the adsorbate layer rotates by an angle β such that the resulting incommensurate moiré superlattice is either oriented along a high-symmetry direction of the substrate or along a high-symmetry direction of the adsorbate layer. Numerical calculations showed that these situations correspond to an energy minimum, since the number of adsorbates in or close to low-energy sites is maximized.[34,35,36] The maximization is solely due to a finite-size effect, with relaxation only resulting in a second-order correction.

In Figure 5 the rotation angle β of the CO lattice with respect to the Pt substrate as a function of the lattice misfit $(d_A - d_S)/d_S$ is compared to the high-symmetry (30 and 60°) solutions relevant for the (111) surface. For comparison, we also show, marked NM, the theoretical harmonic approximation[37] solution

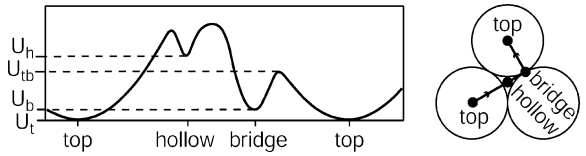

Figure 6. Qualitative potential energy curve for an isolated CO molecule on Pt(111) along the lines connecting the top, bridge and hollow sites.

derived for a Lennard-Jones system in refs 26 and 29. (The longitudinal and transverse sound velocities c_L and c_T are the only system parameters which enter into the solution. For a two-dimensional hexagonal lattice they are related to each other by $c_L = \sqrt{3}c_T$.) For misfit values between 0.3 and 0.4, i.e., coverages below 0.6 monolayers, the experimental data points are found to be in good agreement with the $\Psi_S = 30°$ solution found from the high-symmetry hypothesis, i.e., the moiré vector aligns with the 30° high-symmetry direction of the substrate (which corresponds to the $[1\bar{2}1]$ direction). For misfit values lower than 0.3, however, a deviation from the theoretical lines is observed. As the compression of the CO layer continues, i.e., for lower values of $(d_A - d_S)/d_S$, β remains constant at approximately 10° within the error bars, whereas Ψ decreases from 30° to about ±24° (cf. Figure 3b).

The alignment of the moiré vector with the 30° substrate direction indicates that the particular rotation of the adsorbate layer is due to the finite size of the substrate.[35,36] The role of the substrate boundaries is played by the substrate steps, which are oriented along the $[1\bar{1}0]$ and equivalent directions. It would be interesting to confirm this result in experiments using samples with varying step density.

As established above, the moiré vector does not align with any of the substrate high-symmetry directions at pressures above 10^{-2} Torr. The energy gain associated with this transition (see discussion below) thus does not give a sufficiently high impetus to achieve the rotation. We can analyze the situation in further detail by taking the form of the substrate interaction potential U and the strength of the lateral interaction V_l into account. The exact form of V_l has not yet been determined (see refs 38−41), but an approximation is given by the semiempirical CO−CO pairwise interaction potential in ref 42. A qualitative sketch of U is given in Figure 6, and Table 1 reproduces some potential parameters, derived from the semiempirical single-molecule potential curve[43] of ref 42. The top sites are energetically most favorable, followed by the bridge sites.[3−5] Here we assume that the maximum of the potential energy barrier U_{tb} between top and bridge sites lies below the local potential energy minimum U_h at hollow sites, in agreement with the calculations in ref 38 and the experimental findings of ref 11. As a consequence, the hollow sites are not occupied over the entire investigated pressure range, in agreement with the results of ref 11. The observation of a hexagonal superstructure is not contradicted, since we expect the positions of the adsorbed CO molecules to be relaxed with respect to a perfect hexagonal overlayer. In addition, the area of the near-hollow sites amounts to a relatively small fraction of the total surface area only, so that these sites do not necessarily have to be occupied in a close-to-hexagonal overlayer.

Relevant for a comparison of the lateral interaction energy and the corrugation of the substrate potential are the barriers between the different sites. In the analysis, we have to take into account that the measurements are carried out at room temperature. A crude estimation for the effective barrier height is derived by assuming parabolic and isotropic oscillators. The resulting values for the effective barriers between the bridge

TABLE 1: Parameters of the Employed Substrate Interaction Potential and the Lateral Interaction (All Energies Are Given in meV)[a]

T(K)	U_t	U_b	U_{tb}	$\langle U_t \rangle$	$\langle U_b \rangle$	$\Delta U_{tb-t} \equiv U_{tb} - \langle U_t \rangle - U_t$	$\Delta U_{tb-b} \equiv U_{tb} - \langle U_b \rangle - U_b$	$V_l(\theta = 0.5)$	$V_l(\theta = 0.6)$
0	0	60	300	6	37	294	203	200	290
300	0	60	300	72	60	248	180	200	290

[a] ΔU_{tb-t} and ΔU_{tb-b} represent effective barrier heights relative to the mean energy of the molecule inside the potential wells, which were assumed to be parabolic. These effective barrier heights are derived assuming isotropic oscillators with energies $\langle U_{t,b} \rangle = \hbar\omega_{t,b} + \hbar\omega_{t,b}/(\exp(\hbar\omega_{t,b}/kT) - 1)$, where $\hbar\omega_t = 48$ cm^{-1} and $\hbar\omega_b = 300$ cm^{-1} are the vibrational motion frequencies in the top and bridge positions, respectively.[42] The values defining the potentials (U_t, U_b, U_{tb}, and V_l) have been taken to be temperature independent.

and on-top sites, $\Delta U_{tb-t} \equiv U_{tb} - \langle U_t \rangle - U_t$, as seen from the on-top potential-energy minimum and $\Delta U_{tb-b} \equiv U_{tb} - \langle U_b \rangle - U_b$ as seen from the bridge minimum, are given in Table 1. ΔU_{tb-t} and ΔU_{tb-b} represent the room-temperature effective barrier heights relative to the mean energy of the molecule inside the potential wells (see the Table caption), which were assumed to be parabolic, while U_t, U_b, and U_{tb} are the parameters of the potential energy surface for the on-top and bridge sites and the barrier between these (cf. Figure 6).[42] For the on-top sites, the lateral repulsion energy V_l is smaller than the barrier height ΔU_{tb-t} at the onset of the high-symmetry moiré phase with $\theta \approx 0.5$. At $\theta \approx 0.6$, corresponding to the rotational transition at 10^{-2} Torr, V_l is essentially equal to ΔU_{tb-t}. In contrast, the barrier as seen from the bridge sites, ΔU_{tb-b}, is found to be smaller than the lateral repulsion V_l over the entire coverage range of 0.5−0.6. This indicates that the occupation of top sites is decisive for the formation of the high-symmetry moiré phase at lower CO pressures.

At pressures above 10^{-2} Torr, the orientation of the moiré superstructure along the high-symmetry direction $\Psi = 30°$ is not maintained. Hence, the rotation concomitant with such an alignment is not favorable anymore, and instead, the CO adsorbate layer keeps a constant orientation with respect to the substrate. In this pressure regime, the lateral repulsion exceeds the barrier height between the on-top and bridge position, irrespective of whether these are measured with reference to the bridge (ΔU_{tb-b}) or on-top site (ΔU_{tb-t}). Hence the tendency of the CO molecules to occupy (near) top sites is reduced. We therefore propose that the increasing dominance of the lateral repulsion over the barrier height ΔU_{tb-t} causes the deviation from the high-symmetry direction just above 10^{-2} Torr.

However, close to 760 Torr, the occupation of top sites again becomes decisive, namely, for the formation of a commensurate ($\sqrt{19} \times \sqrt{19}$) R23.4°-13CO structure. In this commensurate structure, a very high number of CO molecules can sit exactly on top sites. We note that the electrochemical study of Villegas and Weaver[11] indicates that going from a negative to a slightly positive sample bias leads to a switching from a (2 × 2)-3CO structure to the ($\sqrt{19} \times \sqrt{19}$) R23.4°-13CO system. The rotation concomitant with such a transformation indicates an enhanced stability of the ($\sqrt{19} \times \sqrt{19}$) structure. Together with the present results, this finding suggests that the occupancy of a high number of on-top sites to some extent can outweigh the lateral repulsion even at high coverages.

The energy gain due to the formation of the commensurate ($\sqrt{19} \times \sqrt{19}$) R23.4°-13CO structure is judged to be higher than the energy gain that would result from a reorientation of the incommensurate moiré superstructure along $\Psi = 30°$ just above 10^{-2} Torr. We suggest that above 10^{-2} Torr the lateral forces are sufficient to exceed the corrugation of the substrate potential. Hence a simple reorientation along a high-symmetry direction is prevented but not the formation of a particularly stable commensurate structure.

Summary

In conclusion, we have determined the room-temperature surface structure of CO on Pt(111) over the entire pressure range of 10^{-6}−760 Torr. For all pressures, the formation of a hexagonal or quasihexagonal CO overlayer is observed, showing that for CO/Pt(111) a true pressure gap cannot be established. Nevertheless, extreme care has to be taken when relating UHV results to systems operating under realistic conditions such as atmospheric pressure. One has to consider (a) the existence of different commensurate vacuum structures on cooled samples (see, e.g., refs 3 and 4) and (b) the subtle differences between the reported hexagonal structures in terms of the adsorbate layer rotation angle.

In further detail, the CO adsorbate layer is continuously compressed with increasing pressure, resulting in a continuous coverage variation from 0.5 to 0.7. The orientation of the moiré superlattice, whose formation is due to the superposition of the hexagonal adsorbate layer with the hexagonal substrate, is pressure dependent. First, for coverages between ∼0.5 and 0.6, the moiré pattern is rotated by 30° with respect to the [1$\bar{1}$0] direction of the Pt(111) substrate. The orientation can be explained in terms of a maximum occupation of high-binding energy sites for a substrate of finite size,[35,36] where the size is given by the surface terraces. Second, at a coverage of 0.6, the system undergoes a rotational phase transition. Above this coverage, the rotation angle of the adsorbate layer with respect to the substrate does not change anymore. We explain this behavior in terms of an increasing importance of the repulsive lateral molecular interaction, which starts to dominate over the corrugation of the substrate interaction potential. A quantitative analysis based on previous results[42] supports our explanation.

References and Notes

(1) *Handbook of Heterogeneous Catalysis*; Ertl, G., Knözinger, H., Weitkamp, J., Eds.; Wiley-VCH: Weinheim, 1997; Vols. 1−5.
(2) See, e.g., ref 1, Vol. 4, p 2094.
(3) Ertl, G.; Neumann, M.; Streit, K. M. *Surf. Sci.* **1977**, *64*, 393.
(4) Persson, B. N. J.; Tüshaus, M.; Bradshaw, A. M. *J. Chem. Phys.* **1990**, *92*, 5034.
(5) McEwen, J.-S.; Payne, S.; Kreuzer, H. J.; Kinne, M.; Denecke, R.; Steinrück, H.-P. *Surf. Sci.* **2003**, *545*, 47.
(6) Su, X.; Cremer, P. S.; Ron Shen, Y.; Somorjai, G. A. *Phys. Rev. Lett.* **1996**, *77*, 3858.
(7) Jensen, J. A.; Rider, K. B.; Salmeron, M.; Somorjai, G. A. *Phys. Rev. Lett.* **1998**, *80*, 1228.
(8) Ertl, G. *Angew. Chem., Int. Ed. Engl.* **1990**, *29*, 1219.
(9) Rupprechter, G.; Dellwig, T.; Unterhalt, H.; Freund, H.-J. *J. Phys. Chem. B* **2001**, *105*, 3797.
(10) Kruse Vestergaard, E.; Thostrup, P.; An, T.; Lægsgaard, E.; Stensgaard, I.; Hammer, B.; Besenbacher, F. *Phys. Rev. Lett.* **2002**, *88*, 259601.
(11) Villegas, I.; Weaver, M. J. *J. Chem. Phys.* **1994**, *101*, 1648.
(12) Biberian, J. P.; van Hove, M. A. *Surf. Sci.* **1984**, *138*, 361.
(13) Here we define the coverage θ as the number of CO molecules per substrate surface atom.
(14) Besenbacher, F. *Rep. Prog. Phys.* **1996**, *59*, 1737.
(15) Lægsgaard, E.; Österlund, L.; Thostrup, P.; Rasmussen, P. B.; Stensgaard, I.; Besenbacher, F. *Rev. Sci. Instrum.* **2001**, *72*, 3537.

(16) Note that the observation of a moiré pattern in STM in general is due to a combination of electronic and geometric effects. In fact, it has been argued that the imaging of moiré patterns in STM is not due to the modulation of the topography, but to (three-dimensional) tunneling from the buried interface.[17] In this model, the enhanced visibility of the moiré pattern is explained in terms of the larger decay length of the long-periodicity wave function, which is associated with the moiré lattice and which is produced by multiple scattering. The exact imaging mechanism is not important in the present context though, since the presence of a moiré pattern unambiguously proves the presence of a (nearly) hexagonal CO adsorbate layer.

(17) Kobayashi, K. *Phys. Rev. B* **1996**, *53*, 11091.

(18) Ramos, M. M. D.; Stoneham, A. M.; Sutton, A. P.; Pethica, J. B. *J. Phys.: Condens. Matter* **1990**, *2*, 5913.

(19) Thostrup, P.; Kruse Vestergaard, E.; An, T.; Lægsgaard, E.; Besenbacher, F. *J. Chem. Phys.* **2003**, *118*, 3724.

(20) Sprunger, P. T.; Besenbacher, F.; Stensgaard, I. *Chem. Phys. Lett.* **1995**, *243*, 439.

(21) In some cases, the satellites were not visible in the STM. In these cases, and as an additional confirmation to the others, the CO lattice parameters can be inferred from the measured moiré superlattice parameters. From Figure 2b, one can derive the following formula:

$$q_A = (q_S^2 + q_M^2 - 2q_S q_M \cos(\pi - \alpha))^{1/2} \quad (1)$$

$$\sin\beta = \frac{q_M}{q_A}\sin(\pi - \alpha) \quad (2)$$

$$\pi - \alpha = \frac{\pi}{3} - \Psi \quad (3)$$

Ψ is taken to be the smallest positive angle between the substrate and moiré lattices. This set of equations allows a determination of all relevant angles and lattice vectors.

(22) The LEED images observed by Ertl et al.[3] exhibit clear spots at temperatures below and more diffuse spots at room temperature, which points to some degree of overlayer disorder at room temperature. The clear LEED pattern can be recovered by sample cooling, and hence the coverage is the same in both cases ($\theta = 0.5$).

(23) Quiros, C.; Robach, O.; Isern, H.; Ordejon, P.; Ferrer, S. *Surf. Sci.* **2003**, *522*, 161.

(24) Leatherman, G. S.; Diehl, R. D. *Langmuir* **1997**, *13*, 7063.

(25) Steele, W. *Chem. Rev.* **1993**, *93*, 2355.

(26) Novaco, A. D.; McTague, J. P. *Phys. Rev. Lett.* **1977**, *38*, 1286.

(27) Villain, J. *Phys. Rev. Lett.* **1978**, *41*, 36.

(28) Novaco, A. D. *Phys. Rev. B* **1979**, *19*, 6493.

(29) McTague, J. P.; Novaco, A. D. *Phys. Rev. B* **1979**, *19*, 5299.

(30) Shiba, H. *J. Phys. Soc. Jpn.* **1979**, *46*, 1852.

(31) Shiba, H. *J. Phys. Soc. Jpn.* **1980**, *48*, 211.

(32) Villain, J.; Gordon, M. B. *Surf. Sci.* **1983**, *125*, 1.

(33) Grey, F.; Bohr, J. In *Phase Transitions in Surface Films 2*; Taub, H., Torzo, G., Lauter, H., Fain, S. C., Eds.; Plenum Press: New York, 1991; NATO ASI Series, Series B, Physics, Vol. 267, p 83.

(34) Grey, F.; Bohr, J. *Appl. Surf. Sci.* **1993**, *65*−*66*, 35.

(35) Grey, F.; Bohr, J. *Europhys. Lett.* **1992**, *18*, 717.

(36) Bohr, J.; Grey, F. *Condens. Matter News* **1992**, *1*, 12.

(37) Anharmonic extensions of the theory of Novaco and McTague have also been formulated, see refs 27, 28, and 32.

(38) van Beurden, P.; Verhoeven, H. G. J.; Kramer, G. J.; Thijsse, B. J. *Phys. Rev. B* **2002**, *66*, 235409.

(39) Jennison, D. R.; Schultz, P. A.; Sears, M. P. *Phys. Rev. Lett.* **1996**, *77*, 4828.

(40) Brako, R.; Šokčević, D. *Surf. Sci.* **2000**, *469*, 185.

(41) Petrova, N.; Yakovkin, I. *Surf. Sci.* **2002**, *519*, 90.

(42) Schweizer, E.; Persson, B. N. J.; Tüshaus, M.; Hoge, D.; Bradshaw, A. M. *Surf. Sci.* **1989**, *213*, 49.

(43) Ref 44 indicates that for CO/Pt(111) density functional calculations (DFT) deliver *qualitatively* wrong results for the potential-energy surface. While this statement subsequently has been softened[45−48] or disputed,[49] DFT results are not reliable for our purposes, and we have to use results from less advanced methods.

(44) Feibelman, P. J.; Hammer, B.; Nørskov, J. K.; Wagner, F.; Scheffler, M.; Stumpf, R.; Watwe, R.; Dumesic, J. *J. Phys. Chem. B* **2001**, *105*, 4018.

(45) Grinberg, I.; Yourdshahyan, Y.; Rappe, A. M. *J. Chem. Phys.* **2002**, *117*, 2264.

(46) Geschke, D.; Başţuğ, T.; Jacob, T.; Fritzsche, S.; Sepp, W.-D.; Fricke, B.; Varga, S.; Anton, J. *Phys. Rev. B* **2001**, *64*, 235411.

(47) Gil, A.; Clotet, A.; Ricart, J. P.; Kresse, G.; García-Hernández, M.; Rösch, N.; Sautet, P. *Surf. Sci.* **2003**, *530*, 71.

(48) Kresse, G.; Gil, A.; Sautet, P. *Phys. Rev. B* **2003**, *68*, 073401.

(49) Olsen, R. A.; Philipsen, P. H. T.; Baerends, E. J. *J. Chem. Phys.* **2003**, *119*, 4522.